Desalination and Water Treatment
www.deswater.com
doi: 10.1080/19443994.2014.915584

55 (2015) 496–505
June

Taylor & Francis
Taylor & Francis Group

Multivariate optimization of phosphate removal and recovery from aqueous solution by struvite crystallization in a fluidized-bed reactor

Mark Daniel G. de Luna[a], Ralf Ruffel M. Abarca[a,b], Chia-Chi Su[c], Yao-Hui Huang[d], Ming-Chun Lu[c,*]

[a]*Department of Chemical Engineering, University of the Philippines, Diliman, Quezon City 1101, Philippines, Tel. +632 981 8500 (3114); Fax: +632 929 6640; emails: mgdeluna@up.edu.ph, mgdeluna@gmail.com (M.D.G. de Luna)*
[b]*Department of Chemical Engineering and Technology, Mindanao State University—Iligan Institute of Technology, Iligan City 9200, Philippines, Tel. +63 63 221 4056, +63 63 492 1173(188); Fax: +63 63 351 6173; emails: ralfruffel.abarca@g.msuiit.edu.ph, ralfabarca@gmail.com (R.R.M. Abarca)*
[c]*Department of Environmental Resources Management, Chia-Nan University of Pharmacy and Science, No. 60, Sec. 1, Erren Rd., Rende Dist., Tainan 71710, Taiwan, emails: mmclu@mail.chna.edu.tw, u@ms17.hinet.net (C.-C. Su), Tel. +886 6 2660489; Fax: +886 6 2663411; email: mmclu@mail.chna.edu.tw (M.-C. Lu)*
[d]*Department of Chemical Engineering, National Cheng Kung University, No. 1, University Road, Tainan City 701, Taiwan, Tel. +886 6 2757575(62636); Fax: +886 6 234496; email: yhhuang@mail.ncku.edu.tw (Y.-H. Huang)*

Received 19 September 2013; Accepted 12 April 2014

ABSTRACT

Struvite crystallization has been widely studied for phosphate removal and recovery from aqueous systems. In this study, struvite crystallization was carried out in a fluidized-bed reactor. Multivariate optimization was conducted using Box–Behnken design (BBD) with influent pH, influent phosphate concentration, and Mg/P molar ratio as independent variables. The output variables comprised total and dissolved phosphate concentrations, ammonium and magnesium concentrations, and fines concentrations. Experimental values of the total phosphate and dissolved phosphate concentrations ranged from 25.6 to 109.4 mg/L and from 7.6 to 39.3 mg/L, respectively, while the fines concentration varied from 5.2 to 101.6 mg/L. Quadratic mathematical models describing the response behavior of experimental BBD data were generated for total phosphate, dissolved phosphate, and fines concentration. The model *p*-values (<0.0001) were significant and their lack-of-fit *p*-values (>0.05) were insignificant. Numerical optimization of process parameters was conducted to minimize total and dissolved phosphate, ammonium and magnesium concentrations, and fines concentration in the effluent. At influent phosphate concentration of 300 mg/L, the results converged to a set of operating conditions: pH 9.5 and Mg/P = 1.3. The close agreement between the data from the validation experiment and the model-predicted values (relative error < 10%) indicates the robustness of the models.

Keywords: Phosphate removal; Struvite; Crystallization; Fluidized-bed reactor; Box–Behnken design; Multivariate optimization

*Corresponding author.

1. Introduction

The release of nutrients (nitrogen and phosphorus) into recipient waters accelerates the deterioration of water resources [1]. These nutrients, mainly in the form of ammonium and phosphates, abound in wastewater effluents of livestock raising, farming, food and beverage industry, semiconductor manufacturing, and dairy industry [2,3]. Unlike nitrogen, phosphorus is a nonrenewable resource. The current 40 million tons per annum extraction rate of phosphate rocks as P_2O_5 would eventually deplete the approximately 7,000 million tons of economically viable phosphate reserves [4]. At present, nutrient pollution management is no longer limited to safeguarding water bodies from eutrophication but also extends to recovering nitrogen and phosphorus from nutrient-rich wastewaters [5].

Magnesium ammonium phosphate (MAP, $MgNH_4PO_4{\cdot}6H_2O$, struvite) crystallization is a proven technology for nutrient removal and recovery [6–17]. MAP precipitation has been applied in treating human urine [10,11], fertilizer wastewater [12,13], swine wastewater [14,15], semiconductor wastewater [3,9,16], and municipal landfill leachate [17].

The overall performance of struvite crystallization is a function of supersaturation, pH, and concentration of reactants [18]. Optimization of process parameters during struvite crystallization can maximize nutrient recovery from nutrient-rich wastewater and minimize nutrient concentration in the treated effluent. For the multivariable struvite crystallization system, the conventional one-factor-at-a-time strategy is inappropriate because the results do not account for the interaction effects between parameters and the large number of runs required makes this technique costly and time-consuming [19,20]. These problems, however, can be addressed by the application of response surface methodology (RSM), a system of mathematical and statistical strategies based on the fit of a polynomial equation to experimental data [19].

The Box–Behnken design (BBD) is a standard experimental design in RSM [19]. BBD combines $2k$ factorials with incomplete block design resulting in a spherical design. The number of experiments required (N) for BBD is given by Eq. (1) [20,21] where the number of variables and the number of center points are represented by k and C_0, respectively.

$$N = 2k(k-1) + C_0 \tag{1}$$

The aim of the present study was to optimize phosphate removal and recovery during struvite-seeded MAP crystallization in a fluidized-bed reactor using BBD. Design-Expert software version 7.0 (Stat-Ease, Inc., Minneapolis, USA) was used to determine the appropriate model for the system, identify significant process parameters and their interactions, and find the optimal operating conditions of fluidized-bed phosphate crystallization.

2. Methodology

2.1. Chemicals and seed material synthesis

Phosphate solution was prepared from KH_2PO_4 (99%, Panreac) crystals and the precipitant solution was prepared from NH_4Cl (99.8%, Merck) powder and $MgCl_2{\cdot}6H_2O$ (99%, Panreac) crystals using reverse osmosis (RO) water.

MAP seed crystals were synthesized in a semi-batch process. In a 5-L glass vessel, the phosphate solution and the precipitant solution containing 0.370 M $MgCl_2$ and 0.555 M NH_4Cl were mixed at 300 rpm. Both the phosphate and the precipitant solutions were introduced into the reactor at 1.7 mL/min using peristaltic pumps (Masterflex 7518–00, Cole-Parmer). The pH of the reaction zone was maintained at pH 8.5 by the addition of NaOH (99%, Merck) or HCl (30%, Merck). Solution pH was monitored by a pH/ORP transmitter (PC-310, Shin Shiang Tech Instruments Co., Ltd) The recovered solids were dried at 37˚C for two days and characterized by scanning electron microscopy and X-ray diffraction spectroscopy prior to fluidized-bed crystallization (FBC) experiments.

2.2. Analytical methods

Spectrophotometric analyses of inorganic phosphate ions and ammonium ions were carried out using a UV–vis spectrophotometer (Genesys 20, Thermo Spectronic). Phosphate ion concentration was determined using phosphomolybdenum blue method at 698 nm [22] while ammonium ion concentration was determined by forming an ammonium phenolate complex (indophenol blue method) at 640 nm [23]. Magnesium ion concentration was measured using an atomic absorption spectrophotometer (AAnalyst 200, Perkin Elmer).

2.3. Reactor set-up and struvite crystallization experiments

A 1.35 L cylindrical glass reactor (Fig. 1) with inlet, outlet, and recirculating sections was used as MAP crystallizer. The FBC column was equipped with a pH/ORP meter, a recirculation pump, and two reagent dosing pumps.

The reactor was filled with RO water prior to the addition of 75–840 μm seed crystals. The pH of the

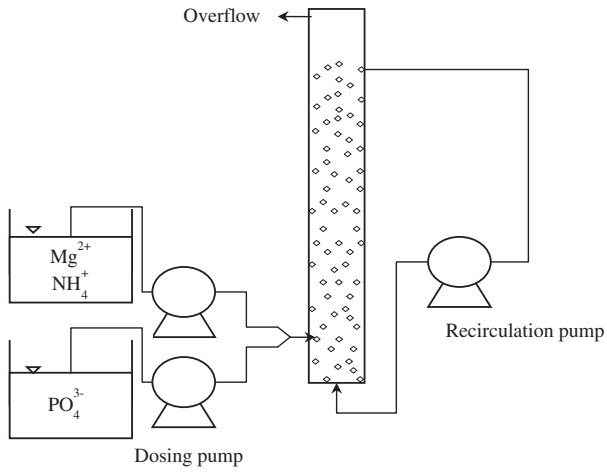

Fig. 1. FBC set-up.

Table 1
Design of experiment for the FBC of struvite

Factors	Symbol	Levels −1	0	+1
Influent pH	A	9.0	9.5	10.0
Initial phosphate conc. (mg/L)	B	100	300	500
Mg/P molar ratio	C	1.0	1.5	2.0

precipitant solution and that of the phosphate solution were adjusted before dosing at 6.0 mL/min. The system operated at ambient temperature of 25℃. Samples were taken from the recirculating liquid at predetermined time intervals. Filtered (using 0.45 μm membrane) and unfiltered samples were mixed with 30 μL concentrated HNO_3 (65%, Merck) prior to phosphate analyses.

The effects of influent pH, influent phosphate concentration and Mg/P molar ratio on residual phosphate, magnesium and ammonium concentrations, and fine crystal (≤53 μm) concentration were evaluated using BBD. The coded and actual levels of the independent variables are shown in Table 1.

3. Results and discussion

In every FBC run, fresh RO water, seed crystals, and reagents are introduced into the fluidized bed reactor. The stabilization of the mixture, where the net change of concentration is negligible, was only attained experimentally after the 4th hour. The complete conditions and responses of the 17 BBD experimental runs, inclusive of 5 replicates at the center point, are shown in Table 2. Each BBD data point in Table 2 is the average of ion concentration values, taken every hour from the 4th to 11th hour of continuous fluidization. The total phosphate (sum of dissolved phosphate and fine crystal concentration) and dissolved phosphate concentrations ranged from 25.6 to 109.4 mg/L and from 7.6 to 39.3 mg/L, respectively, while fines concentration varied from 5.2 to 101.6 mg/L. The highest total phosphate and fines concentrations were obtained at pH 10.0, 500 mg/L PO_4^{3-}, and Mg/P = 1.5. The best response for phosphate (low total and dissolved phosphate concentration) and low fines concentrations were observed at pH 9.5, 300 mg/L PO_4^{3-}, and Mg/P = 1.5 and pH 9.0, 300 mg/L PO_4^{3-}, and Mg/P = 1.0, respectively. High pH and high reagent concentration values promote spontaneous homogeneous crystallization [18] as struvite crystallization reaction in Eq. (2) shifts to the production of more MAP crystals. On the other hand, low pH and low reagent concentration values foster low conversion and crystal growth. Intermediate pH and intermediate reagent concentration values will counterbalance conversion and nucleation.

$$Mg^{2+} + HPO_4^{2-} + NH_4^+ + OH^- + 6H_2O \rightarrow MgNH_4PO_4 \cdot 6H_2O + H_2O \quad (2)$$

3.1. Modeling of the responses

The response behavior of experimental data from BBD can be described by mathematical models. The main effects model shown in Eq. (3) [19,20] describes the most important effects of the parameters under consideration. The terms R, β_0, β_i, X_i, and ε pertain to the response, a constant, the coefficients of the linear parameters, the variables, and the random error or noise to the response, respectively.

$$R = \beta_0 + \sum \beta_0 X_i + \varepsilon \quad (3)$$

The factor interactions (FI) model in Eq. (4) [19,20] integrates the coefficients of the interaction parameters - β_{ij} for X_i and X_j for $i < j$ into Eq. (3).

$$R = \beta_0 + \sum \beta_0 X_i + \sum \beta_{ij} X_i X_j + \varepsilon \quad (4)$$

The general second-order model in Eq. (5) [19,20] incorporates the coefficients of the quadratic factors - β_{ij} for $i < j$ into Eq. (4). This model is used when either main effects model or FI model prove to be inadequate to represent experimental data.

$$R = \beta_0 + \sum \beta_0 X_i + \sum \beta_{ij} X_i X_j + \sum \beta_{ii} X_i^2 + \varepsilon \quad (5)$$

Table 2
Design of experiment showing actual factors and response values

				Response						
Run	pH	Influent PO_4^{3-} (mg/L)	Mg/P molar ratio	Total PO_4^{3-} (mg/L)	Dissolved PO_4^{3-} (mg/L)	Fines conc. (mg/L)	Total NH_4^+ (mg/L)	Dissolved NH_4^+ (mg/L)	Total Mg^{2+} (mg/L)	Dissolved Mg^{2+} (mg/L)
1	9.5	500	1.0	52.8	26.8	26.0	105.6	99.8	8.2	6.4
2	9.5	500	2.0	82.0	7.6	74.4	88.0	76.3	136.3	115.9
3	10.0	300	1.0	85.2	33.3	51.4	73.9	63.4	18.9	3.2
4	10.0	300	2.0	78.8	12.7	66.1	84.5	73.9	103.4	57.0
5	9.0	300	1.0	44.5	39.3	5.2	102.1	95.1	9.8	8.9
6	9.0	300	2.0	60.8	13.7	47.2	95.1	70.4	92.0	88.9
7	9.0	100	1.5	52.4	27.2	25.2	62.2	59.9	19.5	15.8
8	9.0	500	1.5	80.4	14.1	66.3	129.1	105.6	74.2	62.0
9	10.0	100	1.5	69.1	24.0	45.2	37.6	35.2	21.6	9.8
10	9.5	300	1.5	25.6	9.8	15.7	73.9	62.4	46.7	45.7
11	9.5	100	2.0	42.3	15.9	26.4	50.5	50.5	26.2	24.3
12	10.0	500	1.5	109.4	7.8	101.6	93.9	70.4	111.1	59.7
13	9.5	100	1.0	44.1	37.9	6.3	37.6	34.0	7.6	6.8
14	9.5	300	1.5	29.0	11.1	17.9	73.9	59.9	43.0	41.5
15	9.5	300	1.5	34.8	11.5	23.4	66.9	52.8	40.5	40.2
16	9.5	300	1.5	28.2	12.9	15.3	73.9	56.3	38.7	38.0
17	9.5	300	1.5	26.4	13.7	12.7	70.4	59.9	37.7	36.5

In this study, quadratic models were suggested by Design-Expert software for all three responses: total phosphate concentration, dissolved phosphate concentration, and fines concentration. Low standard deviation values (<5.4) and R^2 values closer to unity (>0.9820) for all models (Table 3) confirm that the models are accurate. The model equations for total phosphate concentration (C_T), dissolved phosphate concentration (C_D), and fines concentration (C_{Fines}) are shown in Eqs. (6)–(8), respectively. The coded factors A, B, and C in these equations correspond to variables X_1, X_2, and X_3 which denote actual values of influent pH, influent phosphate concentration, and Mg/P molar ratio, respectively. The levels (–1, 0, +1) of the coded factors A, B, and C can be obtained by substituting the numerical values of X_1, X_2, and X_3 into the respective definitions.

$$C_T = 28.79 + 13.05A + 14.59B + 4.66C + 3.07AB - 5.69AC + 7.76BC + 30.54A^2 + 18.49B^2 + 8.01C^2 \quad (6)$$

$$C_D = 11.77 - 1.98A - 6.07B - 11.0C - 0.75AB + 1.08AC + 0.70BC + 4.66A^2 + 1.82B^2 - 8.44C^2 \quad (7)$$

$$C_{\text{Fines}} = 17.01 + 15.04A + 20.66B + 15.64C + 3.83AB - 6.80AC + 7.06BC + 25.88A^2 + 16.66B^2 - 0.42C^2 \quad (8)$$

where

$$A = \frac{X_1 - 9.5}{0.5} \qquad B = \frac{X_2 - 300}{200} \qquad C = \frac{X_3 - 1.5}{0.5}$$

The appropriateness of a model can be further verified by normal plots, residual analysis, the main and interaction effects, the contour plot, and the analysis of variance (ANOVA) statistics. In ANOVA, the error from the model (residual error) is compared with the error from the results of replicated experiments (central points). The non-agreement of experimental data with the predicted values will result in a significant lack of fit [19].

In this study, ANOVA results for the response surface quadratic models are shown in Tables 4–6. The model F-values obtained for total phosphate concentration, dissolved phosphate concentration, and fines concentrations were 46.9, 50.8, and 44.8, respectively. The model p-values (<0.0001) and lack-of-fit p-values (>0.05) for all quadratic models indicate that all quadratic models are significant and their lack-of-fit values are insignificant [24]. Although most terms in

Table 3
Model summary statistics

Source	Std. deviation	R^2	Adjusted R^2	Predicted R^2	
Total phosphate					
Linear	22.69	0.3262	0.1707	−0.0554	
2FI	25.06	0.3673	−0.0123	−0.7746	
Quadratic	4.81	0.9837	0.9627	0.8160	Suggested
Cubic	3.65	0.9946	0.9786		Aliased
Dissolved phosphate					
Linear	6.03	0.7321	0.6703	0.5788	
2FI	6.82	0.7372	0.5795	0.2300	
Quadratic	1.95	0.9849	0.9656	0.8336	Suggested
Cubic	1.51	0.9948	0.9793		Aliased
Fines concentration					
Linear	19.33	0.5966	0.5035	0.3181	
2FI	21.01	0.6334	0.4134	−0.2080	
Quadratic	5.42	0.9829	0.9610	0.8042	Suggested
Cubic	4.02	0.9946	0.9786		Aliased

Table 4
ANOVA for total phosphate

Source	Sum of squares	*df*	Mean square	*F*-value	*p*-value	Prob. > *F*
Model	9767.13	9	1085.24	46.85	<0.0001	Significant
A-Influent pH	1362.68	1	1362.68	58.83	0.0001	Significant
B-Influent PO_4^{3-}conc.	1702.36	1	1702.36	73.49	<0.0001	Significant
C-Mg/P molar ratio	173.82	1	173.82	7.50	0.0289	Significant
AB	37.82	1	37.82	1.63	0.2421	
AC	129.62	1	129.62	5.60	0.0499	Significant
BC	240.87	1	240.87	10.40	0.0146	Significant
A^2	3926.03	1	3926.03	169.48	<0.0001	Significant
B^2	1440.00	1	1440.00	62.16	0.0001	Significant
C^2	270.20	1	270.20	11.66	0.0112	Significant
Residual	162.15	7	23.16			
Lack of fit	108.97	3	36.32	2.73	0.1781	Not significant
Pure error	53.18	4	13.30			
Cor total	9929.28	16				

the quadratic models (Tables 4–6) are significant, the term *AB* is not significant for both total phosphate concentration (Table 4) and fines concentration (Table 6), and can be reduced in Eqs. (6) and (8) to improve the models. Likewise, C^2 for fines concentration (Table 6) and all parameter interaction terms and B^2 for dissolved phosphate concentration (Table 5) can be simplified.

Consistent with the results of ANOVA statistics, the model equations for total phosphate concentration and fines concentration show that all three parameters taken singly (*A*, *B*, and *C*) have positive effects on the response. The influent phosphate concentration, having the largest coefficient of (14.59) and (20.66) for total phosphate concentration and fines concentration, respectively, exerts the greatest influence on the response. For the dissolved phosphate model equation, the negative coefficients of the main parameters indicate an inverse relationship with the response variable.

The high correlation between experimental data and software-generated predicted values based on Eqs. (6)–(8) is evident in Fig. 2 Actual data points are clustered close to the diagonal line (predicted values) confirming the robustness of the quadratic models for total phosphate concentration, dissolved phosphate

Table 5
ANOVA for dissolved residual phosphate

Source	Sum of squares	*df*	Mean square	*F*-value	*p*-value	Prob. > *F*
Model	1740.84	9	193.43	50.83	<0.0001	Significant
A-Influent pH	31.24	1	31.24	8.21	0.0242	Significant
B-Influent PO_4^{3-} conc.	295.00	1	295.00	77.52	<0.0001	Significant
C-Mg/P molar ratio	967.78	1	967.78	254.32	<0.0001	Significant
AB	2.28	1	2.28	0.60	0.4624	
AC	4.69	1	4.69	1.23	0.3037	
BC	1.99	1	1.99	0.52	0.4932	
A^2	91.60	1	91.60	24.07	0.0017	Significant
B^2	13.90	1	13.90	3.65	0.0976	
C^2	300.23	1	300.23	78.90	<0.0001	Significant
Residual	26.64	7	3.81			
Lack of fit	17.49	3	5.83	2.55	0.1937	Not significant
Pure error	9.14	4	2.29			
Cor total	1767.48	16				

Table 6
ANOVA for fines concentration

Source	Sum of squares	*df*	Mean square	*F*-value	*p*-value	Prob. > *F*
Model	11833.47	9	1314.83	44.77	<0.0001	Significant
A-Influent pH	1809.91	1	1809.91	61.63	0.0001	Significant
B-Influent PO_4^{3-} conc.	3414.27	1	3414.27	116.25	<0.0001	Significant
C-Mg/P molar ratio	1958.13	1	1958.13	66.67	<0.0001	Significant
AB	58.60	1	58.60	2.00	0.2007	
AC	184.96	1	184.96	6.30	0.0404	Significant
BC	199.09	1	199.09	6.78	0.0352	Significant
A^2	2820.70	1	2820.70	96.04	<0.0001	Significant
B^2	1169.04	1	1169.04	39.80	0.0004	Significant
C^2	0.74	1	0.74	0.03	0.8782	
Residual	205.59	7	29.37			
Lack of fit	141.05	3	47.02	2.91	0.1641	Not significant
Pure error	64.54	4	16.13			
Cor total	12039.06	16				

concentration, and fines concentration. The relative magnitudes of actual data points are indicated by a color coding scheme. Blue and red colored data points have the lowest and highest numerical values, respectively. Other colors within the visible light spectrum correspond to intermediate concentrations.

3.2. Response surface analysis

The dependence of total phosphate concentration on influent pH, influent phosphate concentration, and Mg/P molar ratio is shown in Fig. 3. These 3D response surface plots and 2D contour plots allow for the optimization of the predicted model equation by visual inspection. From Fig. 3, the highest phosphate removal can be achieved between pH 9.1 and 9.6. This range is within the optimum pH of 9–10 reported by Lee et al. [25]. Phosphate removal by FBC improved with an increase in pH from pH 9.0 but declined beyond pH 9.6. At high pH, ammonium ions are converted to ammonia and are released from the system in gaseous form. In addition, the precipitation of $Mg(OH)_2$ will commence at high pH and compete with MAP formation [26]. In Fig. 3, the highest phosphate removal can be achieved between 100 and 300 mg/L influent phosphate concentration and Mg/P molar ratio between 1 and 2. The saturation index of the solution with respect to MAP precipitates increases with phosphate concentration thereby enhancing the

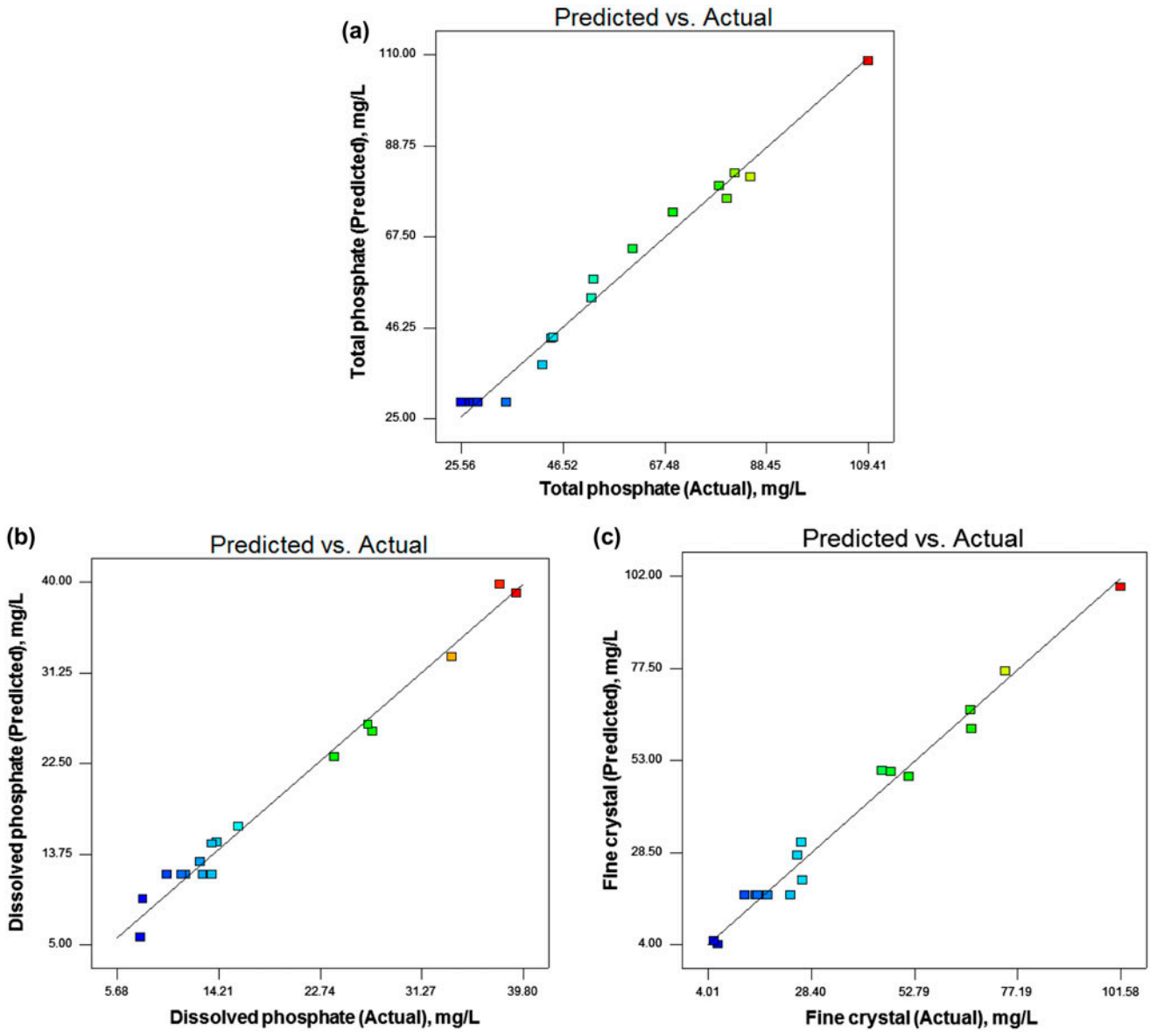

Fig. 2. Distribution of experimentally determined data and model-predicted values of (a) total phosphate (b) dissolved phosphate, and (c) fines concentration.

probability of spontaneous nucleation [27]. Low Mg/P molar ratio prevents the formation of fine crystals but it also lowers the ability of the system to remove phosphate. On the other hand, high Mg/P molar ratio increases the total phosphate concentration due to the formation of fines. In a study on struvite precipitation at varying Mg/P molar ratio, Hirasawa et al. [26] reported that, at Mg/P = 4, fine crystals are formed together with needle-like crystals.

3.3. Numerical optimization and model validation

Numerical optimization of the predicted model equation can be carried out using the desirability function shown in Eq. (9) [20,21] where (d_i) is the desirability of the response and (n) is the number of responses in the measure.

$$D = (d_1 \times d_2 \times d_3, \cdots, d_n)^{1/n} = \left(\prod_{i=1}^{n} d_i\right) \tag{9}$$

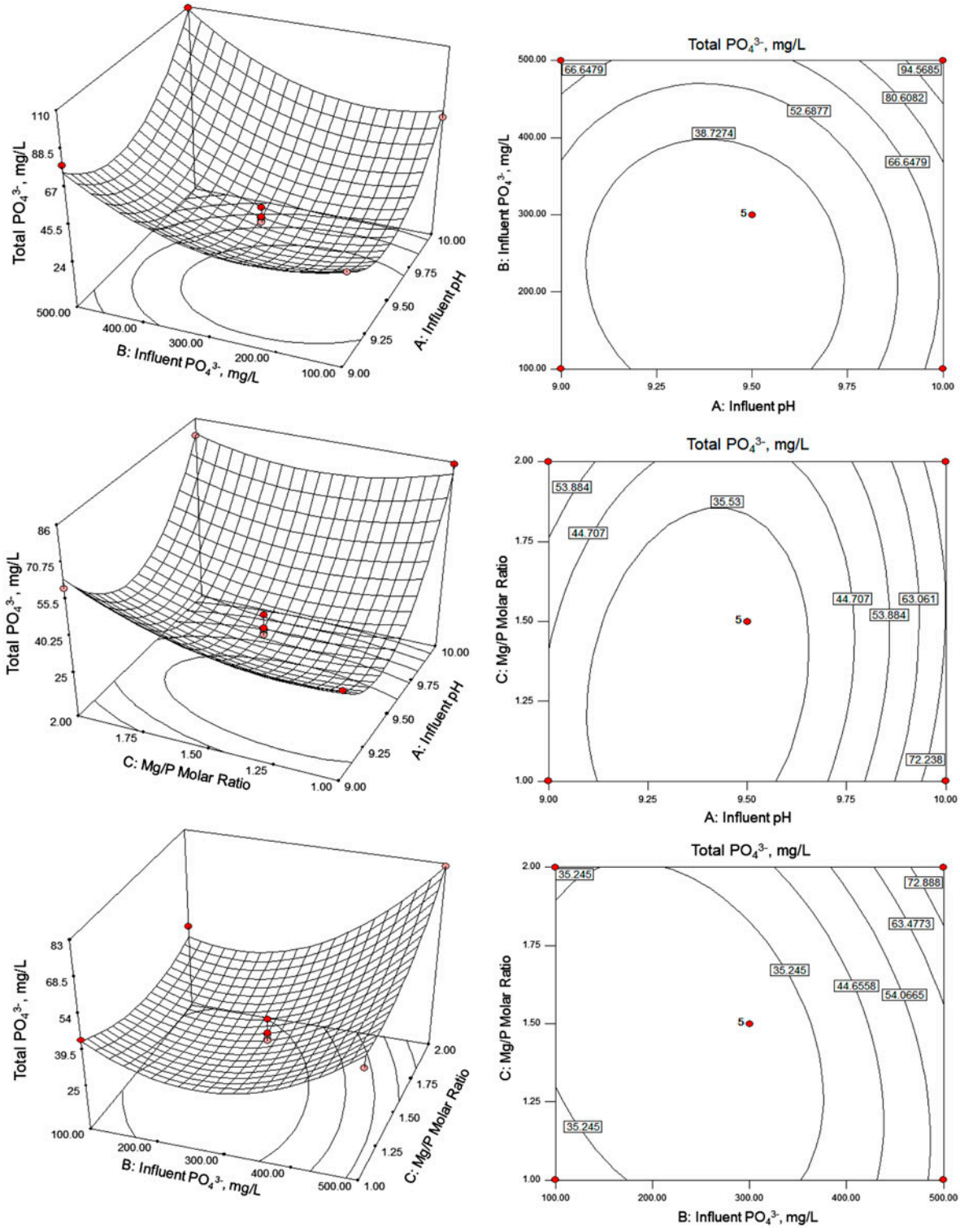

Fig. 3. 3D response surface and 2D contour plots of total phosphate concentration under different combinations of variable parameters.

The desirability function provides the setting of operating parameters that can generate the specified performance level of one or more responses. The values of this function lie between 0 and 1 with 1 being the maximum or the goal. Each parameter setting may be changed to either minimum, maximum, in range, etc. thus effecting subsequent changes to the goal attributes [20,21]. The built-in desirability function in the Design-Expert 7 software was used to compute the optimum values for the independent variables based on predetermined set goals for numerical optimization. Setting influent pH in range, initial phosphate concentration at 300 mg/L, and minimizing Mg/P molar ratio and all other response variables (Table 7) resulted in optimum operating conditions of 9.5, 300 mg/L, and 1.3 for pH, influent phosphate concentration, and Mg/P, respectively. A separate FBC run was conducted using the predicted optimum conditions to validate the results of numerical optimization. The outcome of the verification experiment accounted for the hourly concentrations of individual ions from the 4th to the 11th hour of continuous FBC. Table 8 shows the average values of ion concentrations and the errors relative to the values predicted by numerical optimization. Close agreement is found between the verified and the predicted values. Less than 4% relative error was obtained for phosphate and fines concentrations. While higher relative errors were obtained for ammonium and magnesium concentrations, the values (less than 10%) remain statistically acceptable.

Table 7
Set goals and solution for numerical optimization

Name	Goal	Solution
Independent variables		
Influent pH	Is in range	9.5
Initial phosphate conc. (mg/L)	Equal to 300.0	300
Mg/P molar ratio	Minimize	1.3
Response variables		
Total PO_4^{3-} (mg/L)	Minimize	29.1
Dissolved PO_4^{3-} (mg/L)	Minimize	17.3
Fines concentration (mg/L)	Minimize	11.8
Total NH_4^+ (mg/L)	Minimize	71.7
Dissolved NH_4^+ (mg/L)	Minimize	59.9
Total Mg^{2+} (mg/L)	Minimize	26.5
Dissolved Mg^{2+} (mg/L)	Minimize	25.8

4. Conclusion

Multivariate optimization of struvite-seeded MAP crystallization in a fluidized-bed reactor was carried out using BBD. Setting total and dissolved phosphate, ammonium and magnesium concentrations, and fines concentration in the effluent to minimum, the numerical optimization of process conditions resulted in influent pH of 9.5, 300 mg/L influent phosphate concentration, and Mg/P molar ratio of 1.3. The results of the validation experiment at optimum conditions gave less than 10% error from the model-predicted values indicating that the models were robust and insensitive to noise.

Acknowledgements

The authors would like to thank the National Science Council, Taiwan (Contract No.: NSC 99-2221-E-041-012-MY3) and the Department of Science and Technology, Philippines through the Engineering Research and Development for Technology (ERDT) for financially supporting this research.

Table 8
Experimental values of the responses in verifying the model

Time (h)	Total PO_4^{3-} (mg/L)	Dissolved PO_4^{3-} (mg/L)	Total NH_4^+ (mg/L)	Dissolved NH_4^+ (mg/L)	Total Mg^{2+} (mg/L)	Dissolved Mg^{2+} (mg/L)	Fines conc. (mg/L)
4	29.2	18.5	105.6	70.4	31.6	27.8	10.7
5	28.8	18.5	91.6	73.9	32.4	28.9	10.3
6	29.0	18.1	77.5	63.4	28.6	28.3	10.9
7	28.4	17.7	73.9	66.9	26.4	26.1	10.9
8	28.8	17.3	77.5	70.4	27.8	26.1	11.5
9	29.2	17.5	66.9	63.4	29.4	26.7	11.7
10	29.4	17.1	73.9	59.9	28.6	29.7	12.3
11	29.6	16.7	70.4	56.3	26.9	26.1	12.9
Mean	29.1	17.7	79.7	65.6	29.0	27.4	11.4
Error (%)	0.21	2.02	9.99	8.68	8.60	6.01	3.68

References

[1] L. Pastor, D. Mangin, R. Barat, A. Seco, A pilot-scale study of struvite precipitation in a stirred tank reactor: Conditions influencing the process, Bioresour. Technol. 99 (2008) 6285–6291.

[2] M.I. Ali, P.A. Schneider, An approach of estimating struvite growth kinetic incorporating thermodynamic and solution chemistry, kinetic and process description, Chem. Eng. Sci. 63 (2008) 3514–3525.

[3] H.D. Ryu, C.S. Lim, M.K. Kang, S.I. Lee, Evaluation of struvite obtained from semiconductor wastewater as a fertilizer in cultivating Chinese cabbage, J. Hazard. Mater. 221–222 (2012) 248–255.

[4] L. Shu, P. Schneider, V. Jegatheesan, J. Johnson, An economic evaluation of phosphorus recovery as struvite from digester supernatant, Bioresour. Technol. 97 (2006) 2211–2216.

[5] S. Uludag-Demirer, G.N. Demirer, S. Chen, Ammonia removal from anaerobically digested dairy manure by struvite precipitation, Process Biochem. 40 (2005) 3667–3674.

[6] E.L. Foletto, W.R.B. dos Santos, S.L. Jahn, M.M. Bassaco, M.A. Mazutti, A. Cancelier, A. Gündel, Organic pollutants removal and recovery from animal wastewater by mesoporous struvite precipitation, Desalin. Water Treat. 51 (2013) 2776–2780.

[7] R. Yu, H. Ren, Y. Wang, L. Ding, J. Geng, K. Xu, Y. Zhang, A kinetic study of struvite precipitation recycling technology with $NaOH/Mg(OH)_2$ addition, Bioresour. Technol. 143 (2013) 519–524.

[8] K.S. Le Corre, E. Valsami-Jones, P. Hobbs, B. Jefferson, S.A. Parsons, Agglomeration of struvite crystals, Water Res. 41 (2007) 419–425.

[9] Warmadewanthi, J.C. Liu, Recovery of phosphate and ammonium as struvite from semiconductor wastewater, Sep. Purif. Technol. 64 (2009) 368–373.

[10] B.B. Lind, Z. Ban, S. Byden, Nutrient recovery from human urine by struvite crystallization with ammonia adsorption on zeolite and wollastonite, Bioresour. Technol. 73 (2000) 169–174.

[11] J.A. Wilsenach, C.A.H. Schuurbiers, M.C.M. van Loosdrecht, Phosphate and potassium recovery from source separated urine through struvite precipitation, Water Res. 41 (2007) 458–466.

[12] L. Ouchah, L. Mandi, F. Berrekhis, N. Ouazzani, Essays of phosphorus recovery into struvite from fertilizer industry effluents, Desalin. Water Treat. 51 (2013) 1–7.

[13] N. Hutnik, A. Kozik, A. Mazienczuk, K. Piotrowski, B. Wierzbowska, A. Matynia, Phosphates (V) recovery from phosphorus mineral fertilizers industry wastewater by continuous struvite reaction crystallization process, Water Res. 47 (2013) 3635–3643.

[14] H.D. Ryu, S.I. Lee, Application of struvite precipitation as a pretreatment in treating swine wastewater, Process Biochem. 45 (2010) 563–572.

[15] M.M. Rahman, Y.H. Liu, J.H. Kwag, C.S. Ra, Recovery of struvite from animal wastewater and its nutrient leaching loss in soil, J. Hazard. Mater. 186 (2011) 2026–2030.

[16] H.D. Ryu, D. Kim, S.I. Lee, Application of struvite precipitation in treating ammonium nitrogen from semiconductor wastewater, J. Hazard. Mater. 156 (2008) 163–169.

[17] D. Kim, H.D. Ryu, M.S. Kim, J. Kim, S.I. Lee, Enhancing struvite precipitation potential for ammonia nitrogen removal in municipal landfill leachate, J. Hazard. Mater. 146 (2007) 81–85.

[18] M.I. Ali, P.A. Schneider, A fed-batch design approach of struvite system in controlled supersaturation, Chem. Eng. Sci. 61 (2006) 3951–3961.

[19] M.A. Bezerra, R.E. Santelli, E.P. Oliveira, L.S. Villar, L.A. Escaleira, Response surface methodology (RSM) as a tool for optimization in analytical chemistry, Talanta 76 (2008) 965–977.

[20] V.A. Sakkas, S.A. Islam, C. Stalikas, T.A. Albanis, Photocatalytic degradation using design of experiments: A review and example of the congo red degradation, J. Hazard. Mater. 175 (2010) 33–44.

[21] S.L.C. Ferreira, R.E. Bruns, H.S. Ferreira, G.D. Matos, J.M. David, G.C. Brandao, E.G.P. da Silva, L.A. Portugal, P.S. dos Reis, A.S. Souza, W.N.L. dos Santos, Box–Behnken design: An alternative for the optimization of analytical methods, Anal. Chim. Acta 597 (2007) 179–186.

[22] Z. He, C.W. Honeycutt, A modified molybdenum blue method for orthophosphate determination suitable for investigating enzymatic hydrolysis of organic phosphates, Commun. Soil Sci. Plant Anal. 36 (2005) 1373–1383.

[23] A. Afkhami, R. Norooz-Asl, Micelle-mediated extraction and spectrophotometric determination of ammonia in water samples utilizing indophenol dye formation, J. Braz. Chem. Soc. 19 (2008) 1546–1552.

[24] M.J.K. Bashir, H.A. Aziz, M.S. Yusoff, M.N. Adlan, Application of response surface methodology (RSM) for optimization of ammoniacal nitrogen removal from semi-aerobic landfill leachate using ion exchange resin, Desalination 254 (2010) 154–161.

[25] S.I. Lee, S.Y. Weon, C.W. Lee, B. Koopman, Removal of nitrogen and phosphate from wastewater by addition of bittern, Chemosphere 51 (2003) 265–271.

[26] I. Hirasawa, H. Nakagawa, O. Yosikawa, M. Itoh, Phosphate recovery by reactive crystallization of magnesium ammonium phosphate: Application to wastewater, in: G.D. Botsaris, K. Toyokura (Eds.), Separation and Purification by Crystallization, American Chemical Society, Washington, DC, 1997, pp. 267–276, (Chapter 22), doi: 10.1021/bk-1997-0667.ch022.

[27] Y. Song, H.H. Hahn, E. Hoffmann, Effects of solution conditions on the precipitation of phosphate for recovery: A thermodynamic evaluation, Chemosphere 48 (2002) 1029–1034.